AD

AD-E403 855

Technical Report ARMET-TR-16045

# TWO-DIMENSIONAL STEADY-STATE EDDY CURRENT ANALYSIS OF A SPINNING CONDUCTING CYLINDER

Jyeching Lee
Shana Groeschler

March 2017


U.S. ARMY ARMAMENT RESEARCH, DEVELOPMENT AND ENGINEERING CENTER

Munitions Engineering Technology Center

Picatinny Arsenal, New Jersey

# REPORT DOCUMENTATION PAGE

*Form Approved*
*OMB No. 0704-01-0188*



| 1. REPORT DATE (DD-MM-YYYY) | 2. REPORT TYPE | 3. DATES COVERED (*From - To*) |
|---|---|---|
| March 2017 | Final | February 2013 to August 2014 |

**4. TITLE AND SUBTITLE**

TWO-DIMENSIONAL STEADY-STATE EDDY CURRENT ANALYSIS OF A SPINNING CONDUCTING CYLINDER

5a. CONTRACT NUMBER

5b. GRANT NUMBER

5c. PROGRAM ELEMENT NUMBER

**6. AUTHORS**

Jyeching Lee and Shana Groeschler

5d. PROJECT NUMBER

5e. TASK NUMBER

5f. WORK UNIT NUMBER

**7. PERFORMING ORGANIZATION NAME(S) AND ADDRESS(ES)**
U.S. Army ARDEC, METC
Armaments Engineering Analysis & Manufacturing Directorate (RDAR-MEA-A)
Picatinny Arsenal, NJ 07806

8. PERFORMING ORGANIZATION REPORT NUMBER

**9. SPONSORING/MONITORING AGENCY NAME(S) AND ADDRESS(ES)**
U.S. Army ARDEC, ESIC
Knowledge & Process Management (RDAR-EIK)
Picatinny Arsenal, NJ 07806-5000

10. SPONSOR/MONITOR'S ACRONYM(S)

11. SPONSOR/MONITOR'S REPORT NUMBER(S)
Technical Report ARMET-TR-16045

**12. DISTRIBUTION/AVAILABILITY STATEMENT**
Approved for public release; distribution is unlimited.

**13. SUPPLEMENTARY NOTES**

**14. ABSTRACT**

A spinning metal projectile flying through the magnetic field of earth may generate electromagnetic effects which can disrupt the electronic components contained inside the round. Finite element analyses were conducted to simulate the magnetic field inside a rotating solid conducting cylinder immersed in a uniform transverse magnetic field at steady-state. The factors which affect the magnetic field inside the cylinder were analyzed by varying the angular velocities and the electromagnetic properties (permeability and conductivity) of the cylinder. The response of the magnetic flux density at the center of the cylinder's axis of rotation was also evaluated. The analysis results were compared to the resulting magnetic flux lines on the cylinder of the closed-form theoretical solutions and to the results obtained by the authors in a transient analysis, as presented in a previous paper. The analysis results indicated that the eddy current and skin effect on the magnetic field distribution inside the cylinder was affected by angular velocity and the electromagnetic properties of the cylinder.

**15. SUBJECT TERMS**
Projectile Eddy current Rotating cylinder Finite element analysis (FEA) Spinning Skin affect Magnetic Reynold's number COMSOL

| 16. SECURITY CLASSIFICATION OF: | | | 17. LIMITATION OF ABSTRACT | 18. NUMBER OF PAGES | 19a. NAME OF RESPONSIBLE PERSON |
|---|---|---|---|---|---|
| a. REPORT | b. ABSTRACT | c. THIS PAGE | | | Jyeching Lee |
| U | U | U | SAR | 21 | 19b. TELEPHONE NUMBER (Include area code) (973) 724-2490 |

Standard Form 298 (Rev. 8/98)
Prescribed by ANSI Std. Z39.18

## CONTENTS



## FIGURES

# TABLES

# INTRODUCTION

As military projectiles become more sophisticated, they are becoming increasingly dependent upon electronic devices such as those for sensing and navigation. However, the inclusion of electronic components within a projectile, which is basically a metal cylinder, introduces a variety of electromagnetic effects that need to be accounted for. These effects include induced eddy currents and changes in magnetic flux due to the motion of the projectile. Electromagnetic multi-physics software can be very helpful in understanding these effects, but a background knowledge of electromagnetism is necessary to be able to discern how to set up the analyses and how to evaluate the results and determine whether the results are reasonable. A steady-state analysis was conducted using multi-physics software to better understand the electromagnetic properties inside a rotating conducting cylinder within a magnetic field. Then, to substantiate the analysis outcomes, the results were corroborated through multiple methods.

Induced (eddy) current is generated within a conductor when the conductor moves relative to a stationary magnetic field, such as the magnetic field of earth. The eddy current produces a counter magnetic field and a counter current which tends to cancel the magnetic field within the conductor and also alter the magnetic field outside the conductor. A secondary eddy current and counter magnetic field is induced within the conductor resulting from the changed magnetic field outside the conductor. The entire sequence continues until a steady-state condition is reached. The entire process results in reducing the total magnetic flux within the conductor as described in Lenz's law: The induced (eddy) current produces the magnetic field which tends to oppose the change in magnetic flux that induces such currents, so the total magnetic flux is reduced. Due to the opposing eddy current induced by the changing magnetic field from the alternating current, the skin effect occurs. The skin effect is the tendency of high frequency current and magnetic flux to concentrate near the outer edge, or surface, of a conductor instead of flowing uniformly over the entire cross-sectional area of the conductor, and then to decay toward the center. The higher the frequency, the more pronounced is the skin effect.

## Theoretical Background

This eddy current behavior can be analyzed by using Maxwell-Ampère's law. The magnetic flux density, $\bar{B}$ within the conducting material can be solved using Ampère's equation (refs. 1 to 3), which can be reduced to Bullard's equation as shown in the following steps:
Ampère's equation:

$$\sigma \frac{\partial \bar{A}}{\partial t} + \nabla \times \left( \frac{\bar{B}}{\mu} \right) - \sigma \bar{v} \times \bar{B} = \bar{J}_e \qquad (1)$$

$\sigma$: Conductivity, Siemens/meter (S/m)
$\bar{A}$ : Magnetic vector potential, Weber/meter (Wb/m)
$\bar{B}$: Magnetic flux density, Tesla (T)
$\bar{v}$: Velocity, meter/second (m/s)
$\Omega$: Angular velocity, radian/second (rad/s)
$\mu_0$: Permeability of free space, $4\pi \times 10^{-7}$ Henry/meter (H/m)
$\mu_r$: Relative Permeability of the medium
$\mu$: Permeability of the medium, $\mu = \mu_0 \times \mu_r$ (H/m)
$\bar{J}_e$: External current density, Ampere/meter (A/m)

If there is no external current density,

$$\bar{J}_e = 0 \tag{2}$$

Then, performing a curl operation on Ampère's equation gives,

$$\sigma \frac{\partial(\nabla \times \bar{A})}{\partial t} + \nabla \times \nabla \times \left(\frac{\bar{B}}{\mu}\right) - \nabla \times (\sigma \bar{v} \times \bar{B}) = 0 \tag{3}$$

Maxwell's equation shows the relationship between the magnetic flux density and magnetic vector potential,

$$\bar{B} = \nabla \times \bar{A} \tag{4}$$

And the vector operator identity is,

$$\nabla \times \nabla \times \bar{B} = \lfloor \nabla(\nabla \cdot \bar{B}) - \nabla^2 \bar{B} \rfloor = -\nabla^2 \bar{B} \tag{5}$$

Plugging in equations 4 and 5 into equation 3, reduces equation 3 to Bullard's equation,

$$-\frac{\nabla^2 \bar{B}}{\mu\sigma} = \nabla \times (\bar{v} \times \bar{B}) - \frac{\partial \bar{B}}{\partial t} \tag{6}$$

Since the motion is steady,

$$\frac{\partial \bar{B}}{\partial t} = 0 \tag{7}$$

Bullard's equation 6 reduces to,

$$-\frac{\nabla^2 \bar{B}}{\mu\sigma} = \nabla \times (\bar{v} \times \bar{B}) \tag{8}$$

Bullard's equation shows that the magnetic flux density is a function of velocity, conductivity, and permeability, $\bar{B} = \bar{B}(\bar{v}, \sigma, \mu)$. A closed-form solution, based on Bullard's equation in the steady state condition (eq. 8), was calculated by two researchers to determine the effects of the magnetic field inside and outside a rotating solid conducting cylinder immersed in a uniform transverse magnetic field by varying the angular velocities and the magnetic permeability of the cylinder (ref. 4). Similar studies were conducted by various authors using the analytical method (refs. 5 and 6) and finite element modeling techniques (refs. 7 and 8). A paper previously written by the authors examined these studies and discussed the transient electromagnetic analyses performed to evaluate the electromagnetic effects inside a rotating conducting cylinder (ref. 9). The transient analysis was performed using the electromagnetic field simulation software, ANSYS Maxwell. In contrast to that paper on a transient analysis, the primary analyses being discussed here were conducted in a steady-state condition. The steady state analysis was conducted using COMSOL. Once a transient analysis reaches equilibrium, the response should match the steady-state response. If one is interested in the momentary, dynamic response caused by a change of state, then a transient analysis is necessary. Otherwise, a steady-state analysis is adequate and significantly more time efficient.

The finite element package of COMSOL Multiphysics was used to expand the analytical closed-form analysis performed by Michael P. Perry and Thomas B. Jones (ref. 4). Two-dimensional (2D) finite element steady state analyses of an infinitely long cylinder were modeled. An ambient homogeneous magnetic flux density of 1.0E-5 Tesla was used as input for the analyses. The behavior of the eddy current interaction between the cylinder and the magnetic field excitation was studied in the steady state condition. The magnitude and the phase angle of the magnetic field vector at the center of the cylinder's axis of rotation were also evaluated. The analyses were done in three stages. At each stage, the results of the steady-state analyses were also compared to the transient analyses previously performed and presented by the authors (ref. 9). The stages were as follows:

1) Verify the finite element method by duplicating the analytical analysis on a cylinder performed by Michael P. Perry and Thomas B. Jones (ref. 4).

2) Compare the phase angles of the magnetic flux density at the center of the cylinder for three different conductive materials at various angular velocities in terms of rotational frequencies [3600, 7200, 10800, and 14400 revolutions per minute (rpm)].

3) Conduct a parametric study by varying the relative permeability and the rotational frequencies of the cylinder for a conductive material.

## THE FINITE ELEMENT MODEL

The cylinder and magnetic poles are assumed to be infinitely long with uniform cross sections. The external magnetic field is transverse to the cylinder and there is no induced B (magnetic flux density) in the direction normal to the plane of the cross section. The field patterns in the entire device can be analyzed by modeling the field patterns in its cross section. Therefore, a 2D finite element model was used for the analysis.

Figure 1 shows the two magnetic poles used to generate a constant magnetic field for the cylinder at the center location, the boundary conditions, and the external magnetic field excitation. The tangential components of the magnetic potential are zero at the boundary, n x A = 0, (n = normal vector). The two magnetic poles generate a constant magnetic field of 1.0E-5 Tesla, specified as remanent flux density, $\bar{B}$r. The deformed geometry with the fixed mesh (that retains its original shape as defined by the geometry and original mesh) and prescribed mesh displacement constraint (dx=dy=0) for the entire geometries was modeled (ref. 1).

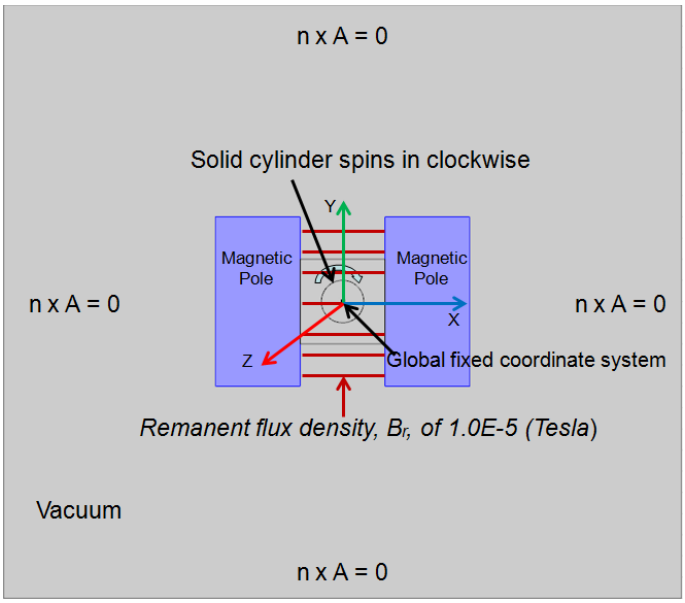


Figure 1
Parts, boundary conditions, and magnetic field excitation

In stage one of the analyses, the analytical analysis results of Perry and Jones (ref. 4) were duplicated using the finite element method with the same boundary conditions (relative permeability and rotating speeds). In stage two, three different material properties were used for the cylinder to study the effects of the electromagnetic properties of the cylinder. Table 1 summarizes the material properties used for the vacuum and for the three materials used for the cylinder in the analysis. In stage three of the analyses, the effects of permeability and rotating speeds of the cylinder on the magnetic field responses of the cylinder were studied. The cylinder was spun in a clockwise rotation with a rotational frequency starting from 3600 rpm and increasing to 14400 rpm, in 3600 rpm increments.

Table 1
Material properties

| Part | Material | Relative Permeability | Relative Permittivity | Electrical Conductivity, S/M | Remanent Flux Density, Tesla |
|---|---|---|---|---|---|
| Magnetic Pole | | 1 | 1 | 1 | 1.0E-5 |
| Case 1 | Structural Steel | 1 | 1 | 4.032E6 | 0 |
| Case 2 | Aluminum | 1 | 1 | 3.774E7 | 0 |
| Case 3 | Copper | 1 | 1 | 5.998E7 | 0 |
| Vacuum | Vacuum | 1 | 1 | 0 | 0 |

## ANALYSIS RESULTS

The purpose of this study was to determine the effects on the magnetic field inside a cylinder immersed in a uniform transverse magnetic field by varying the rotational frequency, electrical conductivity, and magnetic permeability of the cylinder. The magnitude and the phase angle of the magnetic flux density vector at the center of the cylinder were investigated.

### Verification of Finite Element Method

In order to verify the finite element method, stationary analyses were performed to duplicate the closed-form solutions conducted by Michael P. Perry and Thomas B. Jones (ref. 4). The magnetic field inside and outside the cylinder were evaluated based on the following assumptions and summarized in table 2:

- The cylinder motion is steady, $\partial \bar{B}/\partial t = 0$
- The relative permeability of the cylinder($\mu_r$): 1 and 1000
- The conductivity of the cylinder($\sigma$): 3.774E7 S/m (Aluminum)
- Radius of the cylinder($R$): 0.0127 meter
- Magnetic Reynolds number($R_m$), (refs. 3 and 4) : 5 and 25

$$R_m = R^2/\Omega\mu\sigma \tag{9}$$

- Angular velocity($\Omega$): (rad/s)

$$\Omega = R^2/R_m\mu\sigma \tag{10}$$

Table 2
Boundary condition – relative permeability and rotational frequency
(calculated based on Rm)

| Relative Permeability | Magnetic Reynolds Number Rm | Rotational Frequency rpm |
|---|---|---|
| 1 | 5 | 6240 |
| 1 | 25 | 31200 |
| 1000 | 5 | 6.24 |
| 1000 | 25 | 31.2 |

The finite element analysis results indicated that the plots of the magnetic flux lines on the cylinder closely matched that of the closed-form solution for all the cases as shown in figures 2 and 3. These results also closely matched the transient analysis, once steady-state condition was reached, as previously performed by the authors (ref. 9.)

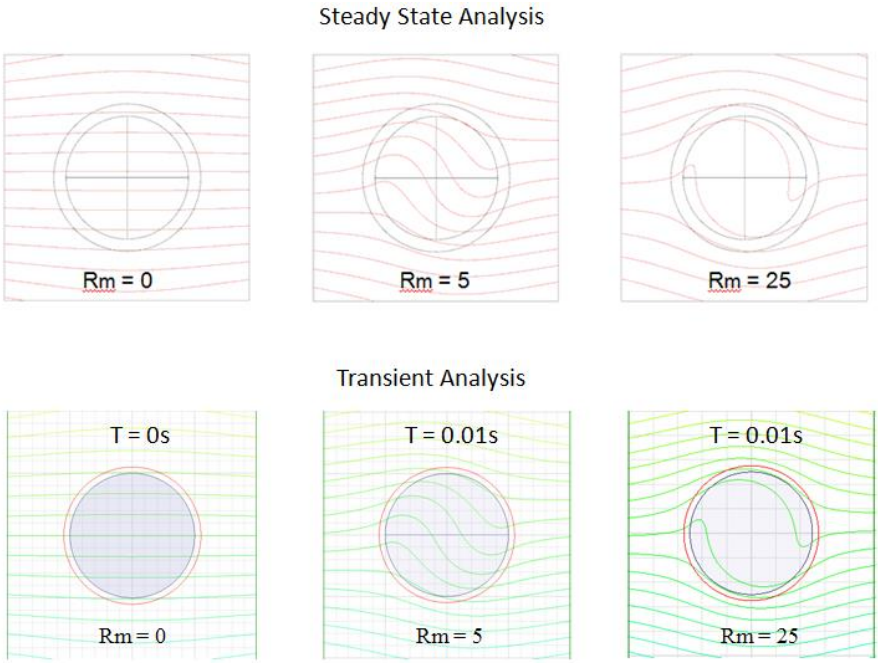


Figure 2
Resulting magnetic flux lines for the cylinder of relative permeability 1.0

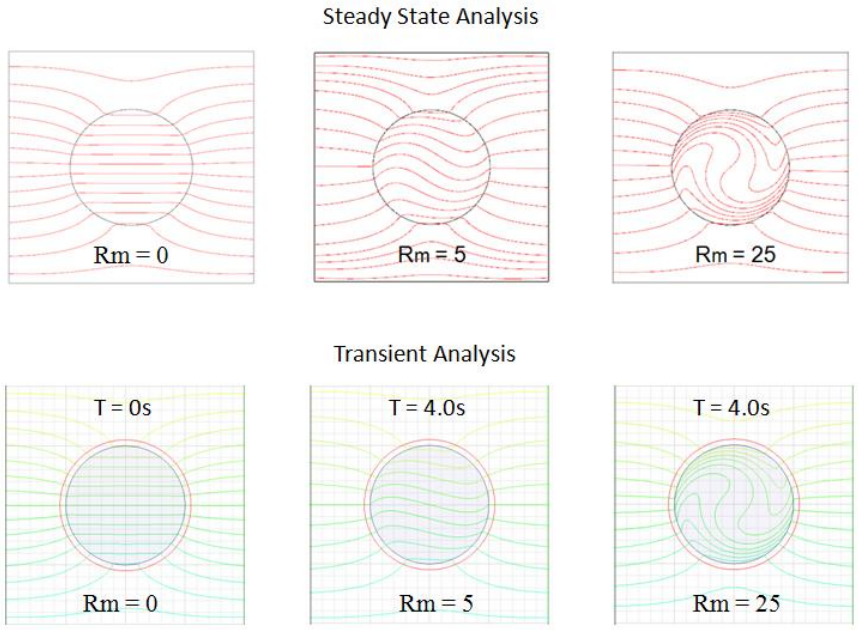


Figure 3
Resulting magnetic flux lines for the cylinder of relative permeability 1000

## Parametrical Study – Electrical Conductivity

Three different conductive materials (structural steel, aluminum, and copper) were chosen to study the effects of the electromagnetic properties of the cylinder. These three materials have the same values for permeability and permittivity except they have different electrical conductivities as shown in the table 1. Steady-state analyses were performed to determine the effect of conductivity on the magnitude and the phase angle of the magnetic flux density vector at the center of the cylinder and the magnetic field distribution inside the cylinder. The cylinder was spun in a clockwise rotation in a range of 3600 to 14400 rpm, in 3600 rpm increments.

The magnetic flux density ($\bar{B}$) is a vector. It has two components for a 2D system. The two components are in the x and y directions ($\bar{B} = \overline{B_x} + \overline{B_y}$). The magnitude ($B_{norm}$) of the magnetic flux density and phase angle ($\theta$) can be calculated as follows and illustrated in figure 4.

$$B_{norm} = \sqrt{{B_x}^2 + {B_y}^2} \tag{11}$$

$$\theta = atan2(B_y, B_x) \tag{12}$$

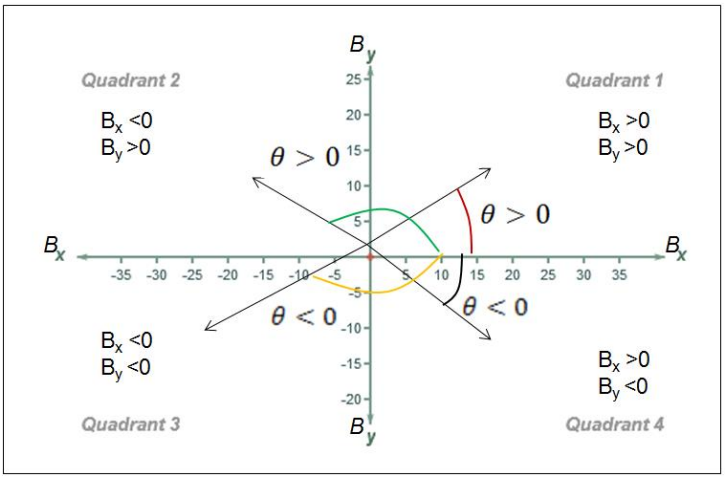


Figure 4
Phase angle and position of the magnetic flux density vector

Because in this analysis the cylinder is rotated in a clockwise direction, the phase angle will also rotate in a clockwise direction, starting from quadrant 4. As is shown in figure 4, when the phase angle increases from quadrant 3 to quadrant 2, the phase angle becomes positive since it is calculated from the shortest route from the positive x axis.

Tables 3 through 5 summarize the magnitude, phase angle, and position, in terms of coordinate quadrant, of the magnetic flux density vector at the center of the cylinder at various rotational frequencies for all three conductive cylinder materials. Comparisons of the magnetic field responses on the structural steel, aluminum, and copper cylinder at various rotational frequencies are shown in table 6. Of the three materials analyzed, the magnitude of the magnetic flux density

vector at the center of the copper cylinder decreased the most while exhibiting the largest phase angles. This is because, of the three materials, copper has the highest conductivity.

Table 3
Magnitude and phase angle of the magnetic flux density vector
at center of structural steel cylinder

| Structural Steel | Center of Rotating Cylinder | | | | |
|---|---|---|---|---|---|
| Rotational Frequency rpm | $B_x$ (Tesla) E-6 | $B_y$ (Tesla) E-6 | $B_{norm}$ (Tesla) E-6 | Phase Angle (deg) | Coordinate Quadrant |
| 3600 | 2.867 | -0.224 | 2.876 | -4.5 | 4 |
| 7200 | 2.829 | -0.443 | 2.864 | -8.9 | 4 |
| 10800 | 2.767 | -0.655 | 2.843 | -13.3 | 4 |
| 14400 | 2.682 | -0.854 | 2.815 | -17.7 | 4 |

Table 4
Magnitude and phase angle of the magnetic flux density vector
at center of aluminum cylinder

| Aluminum | Center of Rotating Cylinder | | | | |
|---|---|---|---|---|---|
| Rotational Frequency rpm | $B_x$ (Tesla) E-6 | $B_y$ (Tesla) E-6 | $B_{norm}$ (Tesla) E-6 | Phase Angle (deg) | Coordinate Quadrant |
| 3600 | 1.977 | -1.639 | 2.568 | -39.7 | 4 |
| 7200 | 0.652 | -1.895 | 2.004 | -71.0 | 4 |
| 10800 | -0.135 | -1.525 | 1.531 | -95.1 | 3 |
| 14400 | -0.497 | -1.079 | 1.189 | -114.7 | 3 |

Table 5
Magnitude and phase angle of the magnetic flux density vector
at center of copper cylinder

| Copper | Center of Rotating Cylinder | | | | |
|---|---|---|---|---|---|
| Rotational Frequency rpm | $B_x$ (Tesla) E-6 | $B_y$ (Tesla) E-6 | $B_{norm}$ (Tesla) E-6 | Phase Angle (deg) | Coordinate Quadrant |
| 3600 | 1.144 | -1.919 | 2.234 | -59.2 | 4 |
| 7200 | -0.224 | -1.444 | 1.461 | -98.8 | 3 |
| 10800 | -0.612 | -0.782 | 0.993 | -128.1 | 3 |
| 14400 | -0.629 | -0.326 | 0.709 | -152.6 | 3 |

Table 6
Comparison of the magnetic field responses on the outside and center of the cylinders at various rotational frequencies

| | Structural Steel | | | Aluminum | | | Copper | | |
|---|---|---|---|---|---|---|---|---|---|
| | Rotating Cylinder | Center of Rotating Cylinder | | Rotating Cylinder | Center of Rotating Cylinder | | Rotating Cylinder | Center of Rotating Cylinder | |
| Rotational Frequency (rpm) | $B_{norm}$ (Tesla) E-6 | $B_{norm}$ (Tesla) E-6 | Phase Angle (deg) | $B_{norm}$ (Tesla) E-6 | $B_{norm}$ (Tesla) E-6 | Phase Angle (deg) | $B_{norm}$ (Tesla) E-6 | $B_{norm}$ (Tesla) E-6 | Phase Angle (deg) |
| 3600 | (2.5 – 3.2) | 2.876 | -4.5 | (2.0 – 3.8) | 2.568 | -39.7 | (1.6 – 4.1) | 2.234 | -59.2 |
| 7200 | (2.5 – 3.2) | 2.864 | -8.9 | (1.4 – 4.3) | 2.004 | -71.0 | (1.0 – 4.6) | 1.461 | -98.8 |
| 10800 | (2.5 – 3.2) | 2.843 | -13.3 | (1.1 – 4.6) | 1.531 | -95.1 | (0.7 – 4.8) | 0.993 | -128.1 |
| 14400 | (2.4 – 3.3) | 2.815 | -17.7 | (0.8 – 4.7) | 1.189 | -114.7 | (0.5 – 4.9) | 0.709 | -152.5 |

Figures 5 to 7 show the magnetic flux density distributions and flux lines for all three conductive materials, respectively. The maximum magnetic flux density responses have a tendency to concentrate at the outer surface of the cylinder with the highest magnitude in the copper cylinder, which has the highest conductivity. The effect increases with rotational frequency. These analyses were also a close match to the transient analysis when the motion has reached the steady-state condition.

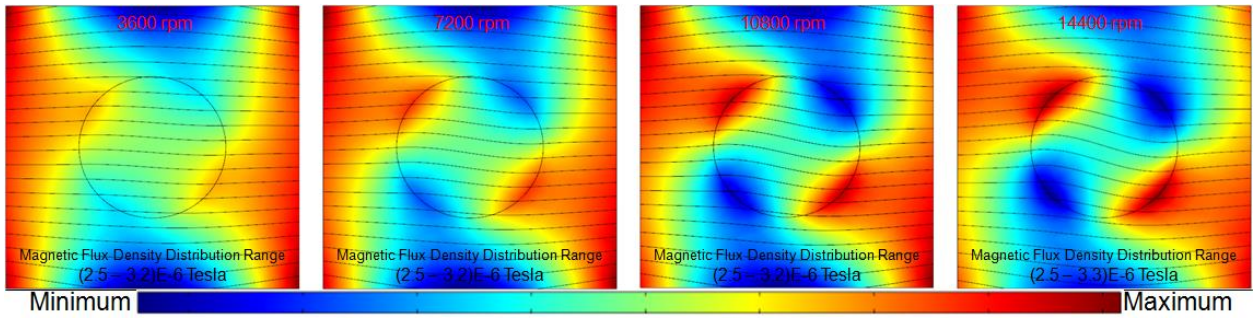


Figure 5
Magnetic flux density distribution and flux lines for structural steel cylinder case

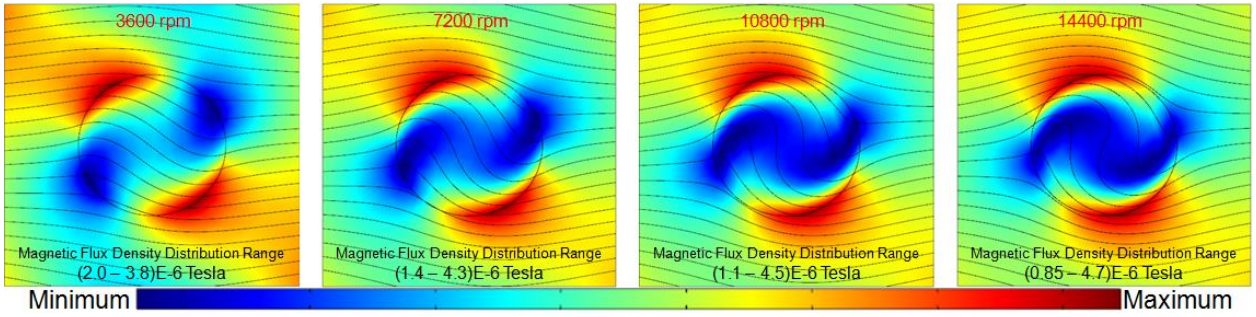


Figure 6
Magnetic flux density distribution and flux lines for aluminum cylinder case

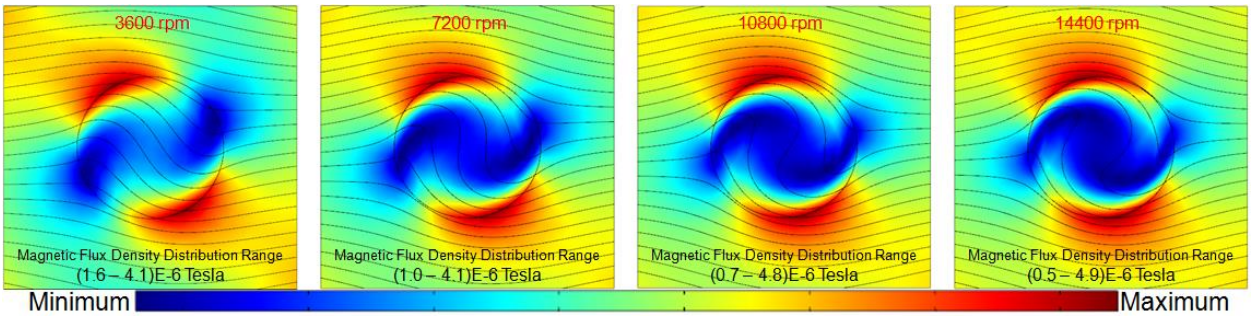


Figure 7
Magnetic flux density distribution and flux lines for copper cylinder case

The analyses results are summarized as follows:

- An increase in conductivity reduces the total magnetic field inside the cylinder as described in Lenz's law.
- An increase in conductivity draws the magnetic field toward to the outer surface of the cylinder due to the skin effect.
- An increase in conductivity decreases the magnitude of the magnetic flux density vector at the center of the cylinder due to the skin effect.
- An increase in conductivity increases the phase angle of the magnetic flux density vector at the center of the cylinder (in this analysis, increasing in a clockwise rotation from quadrant 4).
- The effects on the magnetic field responses inside the cylinder due to eddy currents and skin effect are more pronounced when there is a higher rotational frequency.

### Parametric Study – Magnetic Permeability

The aluminum cylinder was chosen for this study. A parametric study was conducted by varying the relative permeability (from one to six, in increments of one) of the cylinder and spinning it in a clockwise rotation in a range of rotational frequencies, from 3600 to 14400 rpm, in 3600 rpm increments. Figures 8 to 10 show the resulting plots of magnetic flux density and flux lines with varying relative permeabilities and rotational frequencies. Tables 7 to 9 summarize the magnitude and phase angle at the surface and at the center of the cylinder.

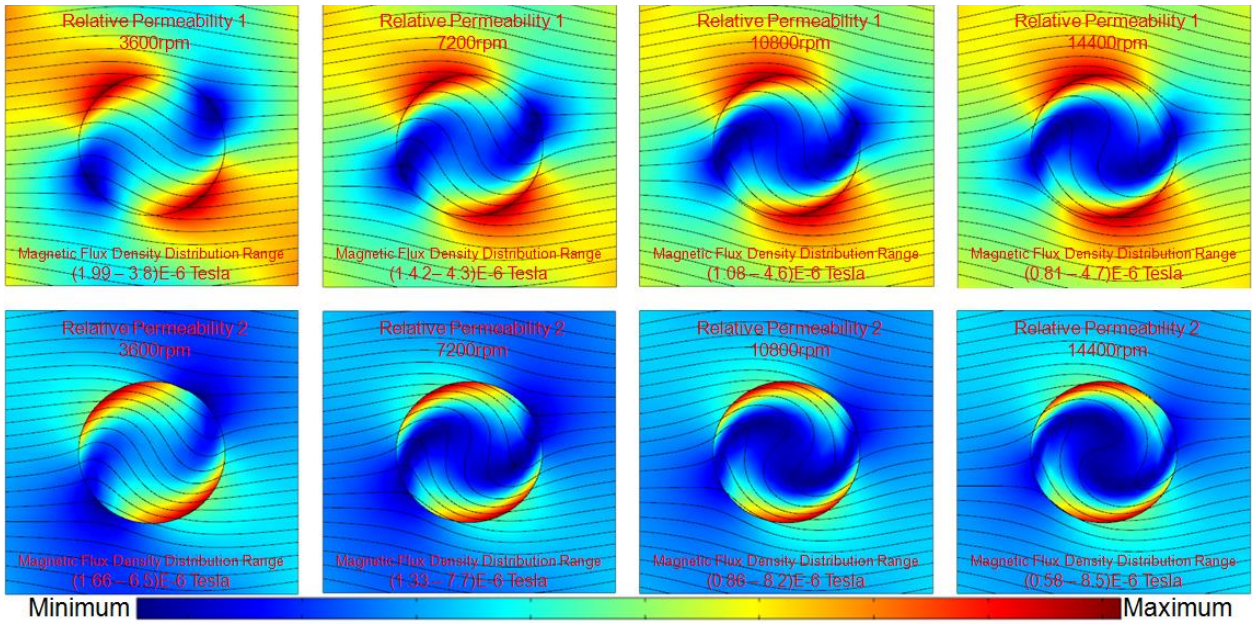


Figure 8
Resulting magnetic flux lines for the cylinder of relative permeability equals 1 and 2

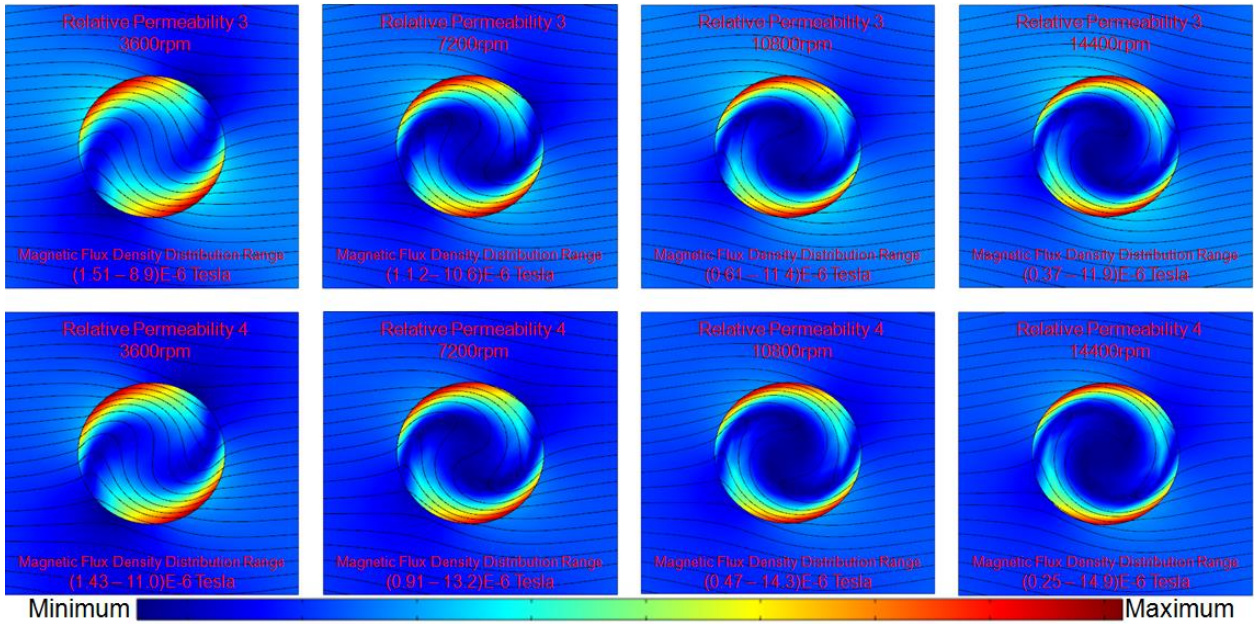


Figure 9
Resulting magnetic flux lines for the cylinder of relative permeability equals 3 and 4

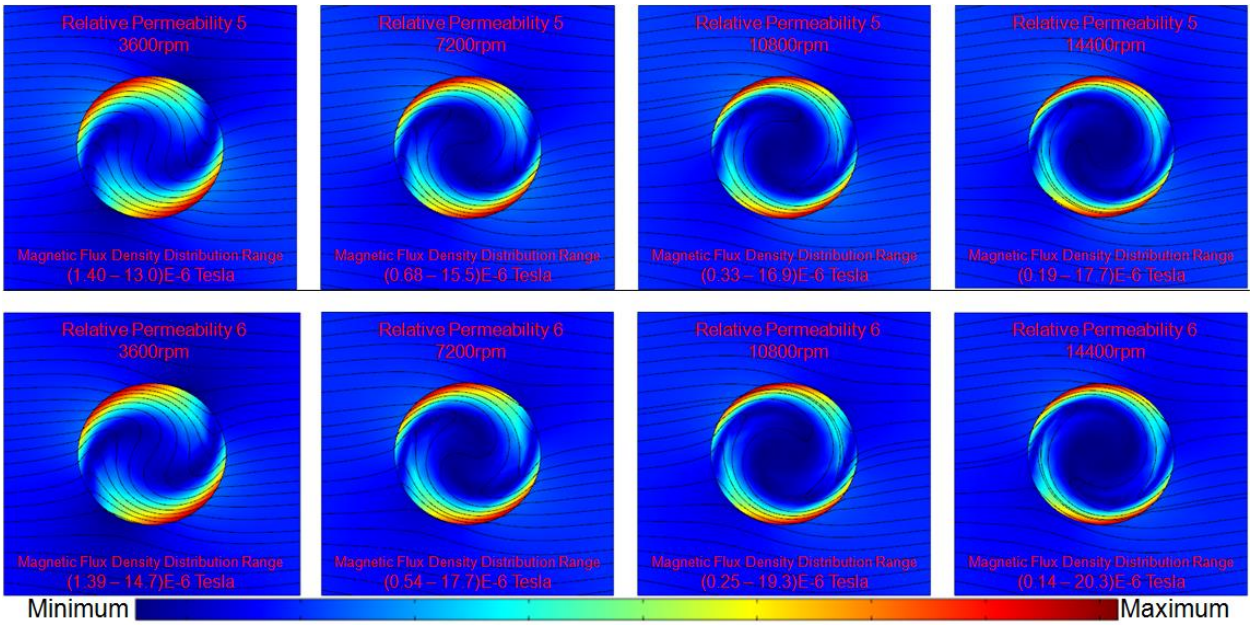


Figure 10
Resulting magnetic flux lines for the cylinder of relative permeability equals 5 and 6

Table 7
Magnitude and phase angle at the surface and the center of the cylinder for relative permeability 1 and 2

| | Relative Permeability 1 | | | | Relative Permeability 2 | | | |
|---|---|---|---|---|---|---|---|---|
| | Rotating Cylinder | Center of Rotating Cylinder | | | Rotating Cylinder | Center of Rotating Cylinder | | |
| Rotational Frequency (rpm) | $B_{norm}$ (Tesla) E-6 | $B_{norm}$ (Tesla) E-6 | Phase Angle (deg) | Coordinate Quadrant | $B_{norm}$ (Tesla) E-6 | $B_{norm}$ (Tesla) E-6 | Phase Angle (deg) | Coordinate Quadrant |
| 3600 | (1.99 – 3.8) | 2.568 | -39.7 | 4 | (1.66 – 6.5) | 2.990 | -63.0 | 4 |
| 7200 | (1.42 – 4.3) | 2.004 | -71.0 | 4 | (1.33 – 7.7) | 1.939 | -106.9 | 3 |
| 10800 | (1.08 – 4.6) | 1.531 | -95.1 | 3 | (0.86 – 8.2) | 1.290 | -140.3 | 3 |
| 14400 | (0.81 – 4.7) | 1.189 | -114.7 | 3 | (0.58 – 8.5) | 0.901 | -168.7 | 3 |

Table 8
Magnitude and phase angle at the surface and the center of the cylinder for relative permeability 3 and 4

| | Relative Permeability 3 | | | | Relative Permeability 4 | | | |
|---|---|---|---|---|---|---|---|---|
| | Rotating Cylinder | Center of Rotating Cylinder | | | Rotating Cylinder | Center of Rotating Cylinder | | |
| Rotational Frequency (rpm) | $B_{norm}$ (Tesla) E-6 | $B_{norm}$ (Tesla) E-6 | Phase Angle (deg) | Coordinate Quadrant | $B_{norm}$ (Tesla) E-6 | $B_{norm}$ (Tesla) E-6 | Phase Angle (deg) | Coordinate Quadrant |
| 3600 | (1.51 – 8.9) | 2.952 | -81.6 | 4 | (1.43 – 11.0) | 2.766 | -97.8 | 3 |
| 7200 | (1.12 – 10.6) | 1.664 | -135.3 | 3 | (0.91 – 13.2) | 1.391 | -160.2 | 3 |
| 10800 | (0.61 – 11.4) | 1.008 | -176.9 | 3 | (0.47 – 14.3) | 0.786 | 151.7 | 2 |
| 14400 | (0.37 – 11.9) | 0.656 | 148.2 | 2 | (0.25 – 14.9) | 0.477 | 112.3 | 2 |

Table 9
Magnitude and phase angle at the surface and the center of the cylinder for relative permeability 5 and 6

| | Relative Permeability 5 | | | | Relative Permeability 6 | | | |
|---|---|---|---|---|---|---|---|---|
| | Rotating Cylinder | Center of Rotating Cylinder | | | Rotating Cylinder | Center of Rotating Cylinder | | |
| Rotational Frequency (rpm) | $B_{norm}$ (Tesla) E-6 | $B_{norm}$ (Tesla) E-6 | Phase Angle (deg) | Coordinate Quadrant | $B_{norm}$ (Tesla) E-6 | $B_{norm}$ (Tesla) E-6 | Phase Angle (deg) | Coordinate Quadrant |
| 3600 | (1.40 – 13.0) | 2.535 | -112.5 | 3 | (1.39 – 14.7) | 2.298 | -126.2 | 3 |
| 7200 | (0.68 – 15.5) | 1.160 | 177.3 | 2 | (0.54 – 17.7) | 0.973 | 156.7 | 2 |
| 10800 | (0.33 – 16.9) | 0.615 | 124.1 | 2 | (0.25 – 19.3) | 0.479 | 99.6 | 2 |
| 14400 | (0.19 – 17.7) | 0.343 | 80.8 | 1 | (0.14 – 20.3) | 0.244 | 51.3 | 1 |

The analyses results are summarized as follows:

- An increase in permeability reduces the total magnetic field inside the cylinder as described in Lenz's law.
- An increase in permeability increases the magnetic field on the outer surface of the cylinder due to the skin effect.
- An increase in permeability decreases the magnitude of the magnetic flux density vector at the center of the cylinder due to the skin effect.
- An increase in relative permeability increases the phase angle of the magnetic flux density vector at the center of the cylinder (keep in mind that in this analysis, the vector starts in quadrant 4 and rotates in a clockwise direction. When the position of the vector rotates to quadrant 2 or quadrant 1 locations, the phase angle becomes positive, so as the phase angle increases, the value of the angle, as calculated from the positive x-axis, becomes smaller).
- The effects on the magnetic field responses inside the cylinder due to eddy currents and skin effect are more pronounced with higher rotational frequency.

## DISCUSSION AND CONCLUSIONS

The electromagnetic analysis of a rotating solid conducting cylinder in a magnetic field was evaluated by comparing the analysis results to the closed form solution and verifying the solutions by comparing the resulting magnetic flux lines on the cylinder. These results also matched the steady-state condition of the transient analysis that the authors previously performed. This correlation was expected since a steady-state analysis should match the results of a transient analysis, once the transient analysis reaches equilibrium. If one is only concerned in the equilibrium condition, a steady-state analysis is more efficient than a transient analysis and can significantly reduce computational resources necessary since it is time independent. In the next stage, a parametric study was performed using a finite element method solver to assess the factors that affect the magnetic field distribution on the cylinder by varying the magnetic material properties (conductivity and permeability) and angular velocity. The magnitude and phase angle of the magnetic flux density vector at the center of the cylinder was investigated.

Bullard's Equation states that the magnetic flux density is proportional to conductivity, velocity, and permeability. The results from the parametric study show that the magnitude and phase angle of the magnetic field vector were affected by the angular velocity and the electromagnetic properties of the cylinder. The analyses results also show the eddy currents and skin effect on the cylinder:

- The eddy currents produce the magnetic flux which tends to oppose the change in magnetic flux that induces such currents, so the total magnetic flux is reduced.
  - The higher the conductivity, the larger the eddy currents are, and the larger the permeability or the higher the rotational frequency, the more pronounced is the magnetic flux reduction.
- The skin effect is the tendency of high frequency current and magnetic flux to concentrate near the outer edge, or surface, of a conductor and then to decay toward the center.
  - The higher the rotational frequency, the larger the magnetic flux at the outer surface of the cylinder.
  - The higher the rotational frequency, the lower the magnetic flux at the center of the cylinder.
- An increase in permeability, conductivity, and rotational frequency produces a larger phase angle of the magnetic flux density vector at the center of the cylinder.

Finite element modeling has been shown to be capable of capturing electromagnetic effects caused by a spinning cylinder within a magnetic field. As more projectiles are being developed containing sensitive electronic components, the ability to model and analyze the magnetic field generated during flight will become more critical in ensuring that the components perform dependably.

## REFERENCES

1. COMSOL AC/DC Module User's Guide, version 4.3a.

2. Perry, Michael P., "Low Frequency Electromagnetic Design," CRC Press; August, 1985.

3. Woodson, H. H. and Melcher, J. R., Electromechanical Dynamics, Part II. New York: John Wiley and Sons, Inc., Chap. 7, pp. 401-405, 1968.

4. Perry, Michael P. and Jones, Thomas B.,"Eddy current Induction in a Solid Conducting Cylinder with a Transverse Magnetic Field," IEEE transactions on Magnetics, vol. MAG-14, no. 4, pp. 227-232, July 1978.

5. Perry, M. P., "Statics and dynamics of ferromagnetic liquid seals" PH.D Thesis, Colorado State University, Ft. Collins, Colorado, August 1976.

6. Van Bladel, J., "Electromagnetic fields in the presence of rotating bodies," Proc. IEEE, vol. 64, no.3, pp. 301-318, 1976.

7. Hwang, J. H. and Lord, W., "Finite Element Analysis of the Magnetic Field Distribution Inside a Rotating Ferromagnetic Bar," IEEE Trans. On Magnetic, vol. MAG-10, no 4, pp. 1114-1118, December 1974.

8. Muramatsu, Kazuhiro, Takahashi, Norio, Iwao, Nobuyuki, Ogawa, Makoto, and Kuwahara, Tohru, "Three-dimensional Steady-State Eddy-Current Analysis of Moving Conductor using Edge Elements and Moving-Coordinate System," IEEE Trans. On Magnetic, vol. 38, no. 2, March 2002.

9. Lee, J. and Groeschler, S., "Transient Simulation of a Rotating Conducting Cylinder in a Transverse Magnetic Field," Technical Report ARMET-TR-15078, U.S. Army ARDEC, Picatinny Arsenal, NJ, September 2016.

## DISTRIBUTION LIST

U.S. Army ARDEC
ATTN: RDAR-EIK
RDAR-MEF-S, J. DeVenezia
RDAR-MEF-E, J. Lee
S. Groeschler
Picatinny Arsenal, NJ 07806-5000

Defense Technical Information Center (DTIC)
ATTN: Accessions Division
8725 John J. Kingman Road, Ste 0944
Fort Belvoir, VA 22060-6218

GIDEP Operations Center
P.O. Box 8000
Corona, CA 91718-8000
gidep@gidep.org